Cell PRESS
Structure
Article

Structural Basis for the PufX-Mediated Dimerization of Bacterial Photosynthetic Core Complexes

Johan Busselez,[1,4] Magali Cottevieille,[2,4] Philippe Cuniasse,[3] Francesca Gubellini,[1] Nicolas Boisset,[2,*] and Daniel Lévy[1,*]
[1]Institut Curie, UMR-CNRS 168, 11 rue Pierre et Marie Curie, F-75231 Paris Cedex 05, France
[2]CNRS, IMPMC-UMR 7590, Paris, F-75005 Paris, France
[3]Commissariat à l'Energie Atomique (CEA), Institut de Biologie et Technologies de Saclay (iBiTecS), Service d'Ingénierie Moléculaire des Protéines (SIMOPRO), Laboratoire de Chimie du Vivant (LCV), Gif-sur-Yvette cedex, F-91191, France
[4]These authors contributed equally to this work.
*Correspondence: daniel.levy@curie.fr (D.L.), nicolas.boisset@impmc.jussieu.fr (N.B.)
DOI 10.1016/j.str.2007.09.026

SUMMARY

In *Rhodobacter (Rba.) sphaeroides*, the subunit PufX is involved in the dimeric organization of the core complex. Here, we report the 3D reconstruction at 12 Å by cryoelectron microscopy of the core complex of *Rba. veldkampii*, a complex of ~300 kDa without symmetry. The core complex is monomeric and constituted by a light-harvesting complex 1 (LH1) ring surrounding a uniquely oriented reaction center (RC). The LH1 consists of 15 resolved α/β heterodimers and is interrupted. Within the opening, PufX polypeptide is assigned at a position facing the Q_B site of the RC. This core complex is different from a dissociated dimer of the core complex of *Rba. sphaeroides* revealing that PufX in *Rba. veldkampii* is unable to dimerize. The absence in PufX of *Rba. veldkampii* of a $G_{31}XXXG_{35}$ dimerization motif highlights the transmembrane interactions between PufX subunits involved in the dimerization of the core complexes of *Rhodobacter* species.

INTRODUCTION

In purple photosynthetic bacteria, highly organized transmembrane pigment-protein complexes perform absorption of light and its conversion into chemical energy. Two light-harvesting (LH), complexes LH2 and LH1, ensure the collection of light. Then, the excitation energy is funneled toward the special pair (P) of bacteriochlorophylls in the reaction center (RC), followed by an electron transfer from P to the ubiquinone (Q) acceptors Q_A and Q_B. After two photoreactions and the acceptance of two protons by the ubiquinol (QH_2) at the Q_B site, this dissociates from the RC and diffuses into the lipid bilayer. The cytochrome bc_1 complex (cyt bc_1) utilizes QH_2 and oxidized cytochrome c_2 as reductant and oxidant, respectively. The net result is a cyclic electron transfer that promotes the formation of a proton gradient across the membrane, which is used for ATP synthesis by F_1F_0 ATPsynthase.

The description of the bacterial photosynthetic apparatus at the atomic level is nearly complete. Three RC structures (Allen et al., 1987; Deisenhofer et al., 1984; Nogi et al., 2000), two LH2 structures (Koepke et al., 1996; Papiz et al., 1989), and one structure of the cyt bc_1 complex (Berry et al., 2004) are available. The last unsolved component is the core complex in which the conversion of the light energy into charge separation occurs. A 4.8 Å resolution structure of the core complex of *Rhodopseudomonas* (*Rps.*) *palustris* has been obtained by X-ray crystallography (Roszak et al., 2003). Medium- and low-resolution structures of core complexes from several species have been reported from electron crystallography and from atomic force microscopy (for a recent review, see Scheuring et al. [2005a]).

In several photosynthetic species lacking LH2 (*Rhodospirillum* [*Rsp.*] *rubrum*, *Blastochloris* [*Blc.*] *viridis*) or with LH1-like LH2 subunits (*Phaeospirillum molishianum*) as well as in *Rsp photometricum*, core complexes consist of a monomeric assembly of a central RC that is surrounded by a LH1 antenna system. The LH1 assembly is composed of bacteriochlorophyll a molecules (Bchl) that are held rigidly in place by α and β polypeptides, each having a molecular weight of about 6 kDa. In these species, the LH1 assembly is reported to form a closed and elliptical ring of 16 α/β pairs.

The RC is composed of the transmembrane subunits H, M, L and an additional bound cytochrome in some species (e.g., in *Blc. Viridis*). In such core complexes, the quinones exchange between the RC and the cytochrome bc1 complex is proposed to be mediated through LH1 "breathing," which facilitates quinone diffusion through the LH1 ring (Aird et al., 2007; Karrasch et al., 1995).

Additional subunits have also been found to be associated with the LH1 assembly although their functional or structural roles have not been identified yet. For example, a small hydrophobic subunit named Ω has been biochemically characterized but not found in the medium resolution

structures obtained from 2D crystals of the core complex (Ghosh et al., 1994; Jamieson et al., 2002). The single helix subunit W, ~10 kDa, has been found associated with the 15 α/β LH1 ring in the 3D crystal of the core complex *Rps. palustris* (Roszak et al., 2003), but the putative gene has not yet been assigned in the genome of *Rps. palustris*.

Another important subunit that is as yet not structurally assigned is PufX, a ~80 aminoacids polypeptide, found in the core complex of *Rba. sphaeroides* and *Rba. capsulatus* and likely in all *Rhodobacter* species. The structure of PufX from *Rba. sphaeroides* has been solved recently by NMR in organic solvent and modeled both as a bent (Tunnicliffe et al., 2006) and a straight (Wang et al., 2007) helix suggesting possible flexibility. In *Rba. sphaeroides* and *Rba. capsulatus*, PufX has been proposed to be involved in photosynthetic growth and in the fast diffusion of quinones from the Q_B site in the RC to the Qo site in the cyt bc_1 complex (Barz et al., 1995; Francia et al., 1999). PufX is also reported to prevent the formation of a closed LH1 ring, to induce the dimerization of the core complex and to orient the RC within the LH1 antenna system. The resulting core complex in *Rba. sphaeroides* and *Rba. blasticus* forms a dimeric assembly with an S-shaped LH1 surrounding two oriented RC (Jungas et al., 1999; Qian et al., 2005; Scheuring et al., 2004b, 2005b), although a dimer of two C-shaped LH1 has also been proposed (Bahatyrova et al., 2004; Siebert et al., 2004). The number of LH1 α/β pairs is 12 (Scheuring et al., 2004b), 13 (Abresch et al., 2005; Scheuring et al., 2005b), or 14 (Qian et al., 2005), leading to variable dimensions of the opening within the LH1 structure. The precise localization of PufX is under debate. It has been suggested that PufX is within the LH1 assembly at the dimer junction (Scheuring et al., 2004b, 2005b), or close to the inner α ring and the Q_B site of the RC (Qian et al., 2005). Such architecture suggests that the quinone exchange could occur through an "opening" in the LH1 ring or through the PufX subunit. Moreover, as shown by spectroscopic analysis in *Rba. sphaeroides*, both RCs within the dimer are functionally interconnected, allowing excitation transfer between them (Comayras et al., 2005a, 2005b). Finally, PufX is also reported to be involved in the formation of a long-range organization of core complexes in the membrane (Bahatyrova et al., 2004; Frese et al., 2000; Jungas et al., 1999) and in a putative supercomplex involving the cyt bc1 complex and the cytochrome c_2 (Joliot et al., 2005).

In this context, we have recently functionally characterized the photosynthetic apparatus of *Rba. veldkampii*, a *Rhodobacter* strain that has diverged independently from the subgroup of *Rba. sphaeroides* and of *Rba. capsulatus* (Tsukatani et al., 2004). We have shown that the fast exchange of quinones between the RC and the cyt bc1 complex is similar to that of *Rba. sphaeroides*. However, the core complex was found to be monomeric after purification by mild procedures and to contain a PufX subunit associated with the LH1-RC (Gubellini et al., 2006).

Here, we report the 3D reconstruction of this *Rba. veldkampii* core complex by cryoelectron microscopy at 12 Å resolution. This 3D reconstruction allows the determination of the subunits organization of the core complex, including the α/β heterodimers of the LH1 and of the RC (H, M, and L) subunits. The core complex consists of 15 α/β subunits surrounding an oriented RC. The LH1 ring is larger and much less elliptical than the LH1 assembly of the core complexes from other species. Additional densities close to the LH1 assembly and facing the Q_B site of the RC could be assigned to PufX. The sequence analysis of PufX also revealed an absence of a $G_{31}XXXG_{35}$ dimerization motif that is thought to play a crucial role in PufX-PufX transmembrane interactions during oligomerization of the core complexes from *Rhodobacter species*.

RESULTS

3D Reconstruction of LH1-RC from Cryo-Electron Microscopy Images

The core complex from *Rba. veldkampii* was extracted from photosynthetically grown bacteria and purified in n-dodecyl-β-D-thiomaltoside (DOTM), a low cmc detergent. Biochemical analysis by MALDI/MS and by ES Q-tof MS/MS has shown the core complex to consist of the RC proteins H (34.9 kDa), M (31.4 kDa), and L (28.1 kDa), the LH1 subunits α (5.4 kDa) and β (6.7 kDa) as well as PufX (~9 kDa) (Gubellini et al., 2006). Mild solubilization always yielded a monomeric and never a dimeric core complex, suggesting that this is its native oligomeric state. Alignment and classification of negatively stained solubilized core complexes at 25 Å resolution has revealed that the core complex was ~13 nm in diameter and consisted of the LH1 ring surrounding the RC.

We then evaluated the use of a low-pass filtered volume of the core complex of *Rps. palustris* (25 Å resolution), as the first reference for the alignment of cryo-EM images of the core complex of *Rba. veldkampii*. The core complex of *Rps. palustris* is also monomeric, consisted of similar LH1 and RC subunits and of W, a "Puf-like" subunit, and it is the only available structure of a core complex at high resolution. The aim was to bypass the building of a reference volume of such a small, ~300 kDa, globular, and nonsymmetric particle with few distinct features in the top views (white arrow) and in the side views (dark arrow) (Figure 1A). After the first cycle of refinement, cryo-EM images of *Rba. veldkampii* were subsequently iteratively aligned on their own, and the resulting 3D reconstruction of each cycle was used as a reference for the next. Therefore, the volumes diverged from the original reference volume and reached a final resolution of 12 Å, using $FSC_{0.5}$ resolution criterion (Figure 1B). The lack of influence of the original reference on the final 3D reconstruction is clearly illustrated by Figures 1D–1G. For example, when comparing the top view 2D projections of *Rps. palustris* (Figures 1D1 and 1D7) with the similar projections of the final *Rba. veldkampii* 3D reconstruction (Figures 1G1 and 1G7) or the corresponding 2D cryo-EM class average (Figures 1E1 and 1E7), the ellipsoid overall shape of *Rps. palustris* is obvious, while it is clearly circular in *Rba. veldkampii*. Another clear difference is observed in an intermediate orientation (Figures 1D2–1G2), and other orientations also

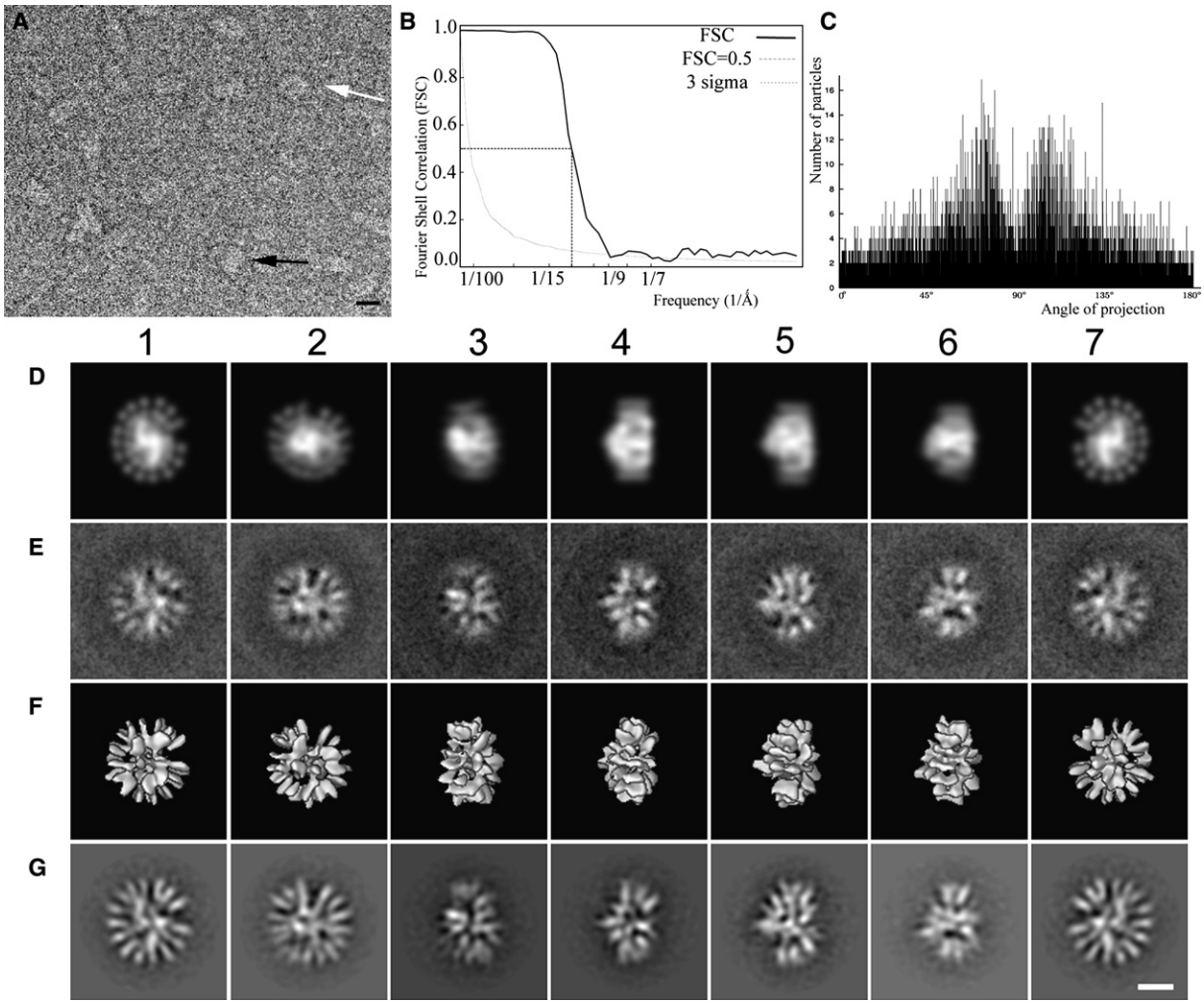

Figure 1. Cryo-EM Analysis of LH1-RC from *Rba. veldkampii*

(A) Micrograph of ice-embedded core complexes of *Rba. veldkampii*. Top view and side view are depicted by white and black arrows, respectively. Scale bar, 10 nm.

(B) FSC plot. The resolution of the 3D reconstruction is estimated to 1/12 $Å^{-1}$ according to the $FSC_{0.5}$ criterion and 1/9.5 Å according to the three sigma criterion.

(C) Angular distribution of the LH1-RC cryo-EM experimental images as a plot of the Euler theta angle where 0°, 90°, and 180° correspond to the top, the side, and the bottom views, respectively.

(D–G) Comparison of the final 3D reconstruction at 1/12 Å resolution with the low pass filtered up to 25 Å volume of the core complex of *Rps palustris* (PDB ID: 1PYH) used as the initial reference volume for the iterative alignment of cryo-EM images of *Rba. veldkampii* (see Experimental Procedures). (D) Set of 2D projection maps from the volume of *Rps palustris*. (E) Set of cryo EM class averages obtained by 3D projection alignment of the experimental cryo EM images on the final 3D reconstruction volume of *Rba. veldkampii*. (F) Oriented 3D surface rendered views of the corresponding projections in the final reconstruction volume. (G) Set of 2D projections of the final 3D reconstruction volume in selected directions of projections matching the class averages in (D). In (D)–(G), each column corresponds to a given set of Euler angles (of identical orientations). Scale bar, 5 nm.

show several significant features that confirm an absence of influence of the initial reference on the final 3D reconstruction (e.g., Figures 1D5 and 1D6 and 1G5 and 1G6). One can also see that central densities, which have a small influence on the alignment process, are very similar (S shaped) in Figures 1D1–1G1, indicating that these densities most likely correspond to similar features (RC) in both species. Conversely, one feature that probably had a strong influence during alignment is the presence of the gap or notch in the LH1 ring (e.g. Figures 1D1–1G1). Indeed, two other volumes without an interruption in the LH1 assembly were also evaluated as references for the 3D projection matching but failed to converge. The first one was built from the volume of the core complex of *Rps. palustris* with an additional LH1 subunit to enclose the LH1 ring, i.e. with 16 α/β subunits. The second one was constructed from a ring of continuous densities, and a central RC low pass filtered to 25 Å, from *Rba. sphaeroides* a related species. This showed that in the initial stage of the refinement the origin of the reference was not important if the overall shape allowed a rough alignment of 2D projections. Here, the absence of a notch in

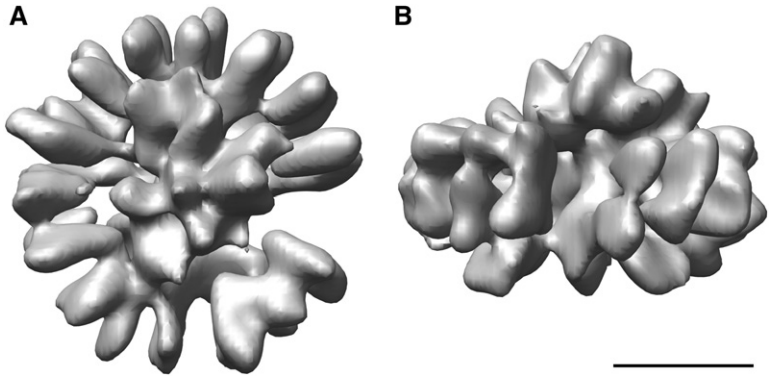

Figure 2. 3D Reconstruction of LH1-RC from *Rba. veldkampii*
(A) Top view of the cytoplasmic side showing the LH1 ring constituted by 15 α/β subunits surrounding the central RC.
(B) Side view highlighting an opening in LH1. Scale bar, 5nm.

the circular ring explained the failure of both "unnotched" references. Finally, particles used for the 3D reconstruction were found to be approximately randomly oriented in the vitreous ice layer (Figure 1C). A slight over representation of the views with elliptical shapes was small enough to have an impact on the isotropy of the final 3D reconstruction.

Subunits Organization of the Monomeric Core Complex

The core complex (Figure 2) is larger and less elliptical than the core complex of *Rps. palustris*. Its diameters are 133 Å along the RC long axis by 129 Å, compared to 120 Å by 110 Å for *Rps. palustris*. The LH1 assembly is ~45 Å high and contains 15 well-resolved α/β heterodimers that surround a central RC. The densities of each α/β heterodimer are 8.5 Å in diameter, consistent with its helical pair structure. The helices within each heterodimer are separated by an average distance of 20 ± 2 Å. The LH1 assembly is interrupted by an opening of 40 ± 1 Å, large enough to allow the insertion of an additional α/β pair.

The RC of *Rba. sphaeroides*, the most closely related species, was fitted in the corresponding densities of the 3D reconstruction (Figure 3). Densities corresponding to the bundles of helices L_A/L_B and $L_C/L_D/L_E$ of subunit L (Figure 3, orange) and helices M_A/M_B and $M_C/M_D/M_E$ of subunit M (Figure 3, purple) were clearly identified in this way. Furthermore the extramembraneous domains including the cytoplasmic domain of the H subunit (Figure 3A, yellow) as well as the periplasmic loops between the helices L_A and L_B and between the helices M_A and M_B were also resolved. Collectively, these features reveal that the RC is uniquely oriented within the LH1 assembly. Indeed, this is demonstrated by the fact that a density could be assigned to the transmembrane helix of the H subunit (Figure 3A, yellow). Furthermore, it is important to note that in this orientation, the Q_B site is facing the gap in the LH1 assembly.

The H, L, and M subunits of the RC and the α/β pairs of LH1 being assigned, we then analyzed the densities that can be attributed to the only subunit not assigned, i.e., the PufX subunit. As shown by several biochemical studies on the core complexes of *Rba. sphaeroides* and of *Rba. capsulatus*, PufX interrupts the LH1 assembly and interacts with the α and not the β subunit (see, e.g., Aklujkar and Beatty [2006] and Parkes-Loach et al. [2004]). In *Rba. veldkampii*, within the opening region (Figure 4), one additional density is found between the α inner ring and the RC (Figure 4A, purple threshold, red ellipse). At a lower threshold, other densities are found to be aligned to the vertical axis of the previous density (Figure 4A, brown threshold, blue and white ellipses). To verify that these discontinuous densities were not from the neighboring α/β subunits, the LH1 densities were manually fitted with the LH1 assembly of *Rps. palustris* constituted by the α/β pairs and the single helix of W subunit. As shown in Figure 4B, the densities of the LH1 close to the opening region of the 3D reconstruction overlap with the corresponding α/β pairs of the LH1 of *Rps. palustris* (green helices). This confirms that they are constituted by α/β heterodimers, while the discontinuous densities correspond to a different subunit. The overlap is progressively lost

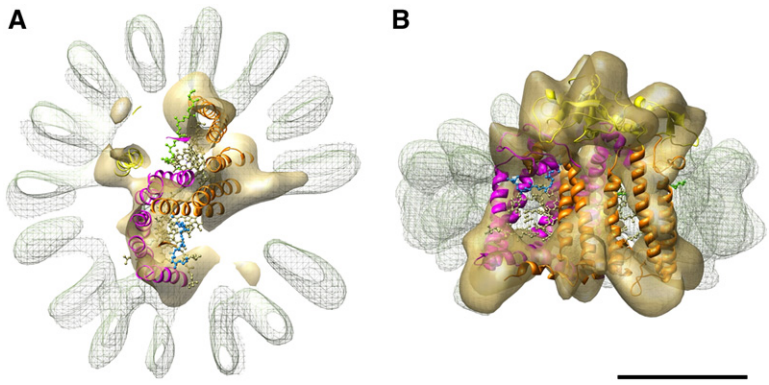

Figure 3. Fitting of the RC of *Rba. sphaeroides* in the Cryo-EM Volume of *Rba. veldkampii*
(A and B) The RC is uniquely oriented within the LH1 ring. The H, L, M subunits of the RC are shown in ribbons: L subunit in orange, M subunit in magenta, and H subunit in yellow. The bacteriochlorophylls special pair in balls and sticks is indicated in light brown, and the quinone Q_B in blue. Note that the Q_B site is adjacent to the gap in the ring.

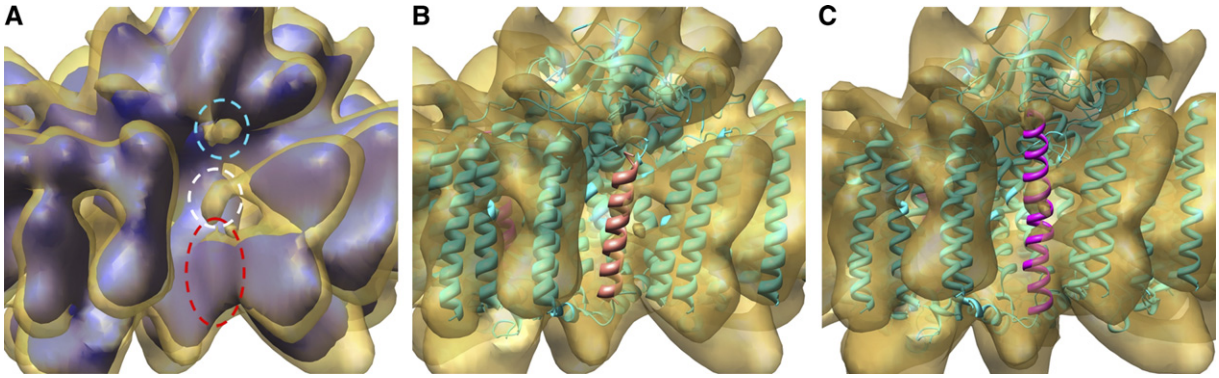

Figure 4. Structural Arrangement of the LH1 Subunits around the Opening Region

Volumes are depicted at two thresholds in purple and in brown. All panels are side views. (A) A high density that can not be assigned to a LH1 or a RC subunit is found close to the α subunit ring within the gap (red ellipse). At a lower threshold, two additional densities are found along the vertical axis of the red density (white and blue ellipses). (B) Fitting of the LH1 assembly with the α/β pairs (green helices) and the W subunit (brown helix) of the core complex of *Rps. palustris* within the volume of the core complex of *Rba. veldkampii*. It is important to note that W is only found in *Rps. palustris* and not in *Rba veldkampii*, and the converse is true for PufX. (C) Same as in B but using the PufX NMR structure from *Rba. sphaeroides* (PDB ID: 2DW3) (purple helix). Note that PufX fits into the three delineated densities (red, white, and blue ellipses).

for the α/β pairs closest to the opening due to the larger diameter of the core complex of *Rba. velkampii* (data not shown). We then manually fitted the PufX subunit of *Rba. sphaeroides* recently determined by NMR (Wang et al., 2007) (Figure 4C, purple helix) that overlaps with the discontinuous densities (Figure 4C) (see discussion). This position close to the ring opening and facing the Q_B site is also consistent with the reported role of PufX in mediating quinone diffusion through the LH1 ring (Comayras et al., 2005a, 2005b; Gubellini et al., 2006). Finally, the location of these densities is close to the position where the W subunit interrupts the LH1assembly in the core complex of *Rps. palustris* (Figure 4B, brown helix, red and white ellipses).

DISCUSSION

The 3D reconstruction of LH1-RC from *Rba. veldkampii* shows several features similar to the core complex of *Rps. palustris*, e.g., the number of α/β pairs and the presence of an opening in the LH1 ring. Since we used a filtered model of LH1-RC of *Rps. palustris* as a first reference for the alignment of the cryo-EM images, we carefully evaluated the final 3D reconstruction to confirm that it was not biased by the reference. Other references constituted by a closed LH1 assembly were tested and did not allow a correct alignment of the images, highlighting the importance of the LH1 opening in the image alignment process. Besides, the shape and dimensions of both core complexes are significantly different, with a much less elliptical and larger core complex of *Rba. veldkampii* (Figures 1D–1G). This divergence appeared after the second cycle of refinement, indicating that the refinement had become independent from the original reference structure. Several methods to generate initial models have been developed by different groups to bypass the use of an initial model built from experimental cryo-images (Baker and Cheng, 1996; Chen et al., 1994; Crowther, 1971; Gelfand and Goncharov, 1989; Leschziner and Nogales, 2006; Ludtke et al., 1999; Radermacher et al., 1987a, 1987b). Starting volumes were in many cases synthetic models and for symmetric objects entire 3D reconstructions strategies now rely on such synthetic references (Yan et al., 2007). The use of homologous atomic models, as we performed here, has already been successfully used (Baker and Cheng, 1996), and its principle can be compared to the molecular replacement method.

The LH1 assembly (Figure 2) with a long axis/short axis ratio R_{axis} of 1.03, is much less elliptical than the core complexes of *Rps. palustris* (R_{axis} of 1.18) (Roszak et al., 2003; Scheuring et al., 2006), of *Rsp. photometricum* (R_{axis} of 1.19) (Scheuring and Sturgis, 2005), or of *Rsp. rubrum* (R_{axis} of 1.19) (Jamieson et al., 2002). The ellipticity of LH1 has been proposed to be induced by interaction of the LH1 assembly with the central RC since recircularization of the empty LH1 ring has been observed by AFM upon RC removal from the native membranes (Scheuring et al., 2003). Here, the LH1 ring appears similar to an "empty ring" or to a LH1 with reduced interactions with the central RC. The larger size of the core complex with a diameter of 133 Å compared to 120 Å for *Rba. sphaeroides* (Scheuring et al., 2004b), 115 Å for *Rsp. rubrum* (Jamieson et al., 2002), or 110 Å for *Rsp. photometricum* (Scheuring et al., 2004a), likely decreases the RC and LH1 interactions. However, the RC is uniquely oriented within the LH1 as shown by the resolved features of the RC (e.g., H subunit, Figure 3A) within the 3D reconstruction. We thus suggest that as shown in the case of *Rba. sphaeroides* (Qian et al., 2005; Scheuring et al., 2004b) and *Rba. blasticus* (Scheuring et al., 2005b), direct interactions of PufX with the RC are involved in the orientation of the RC in *Rba. veldkampii*.

The monomeric state of the core complex of *Rba. veldkampii* in detergent likely corresponds to the in vivo state and did not result from the dissociation of a dimeric core complex upon purification. The monomeric state

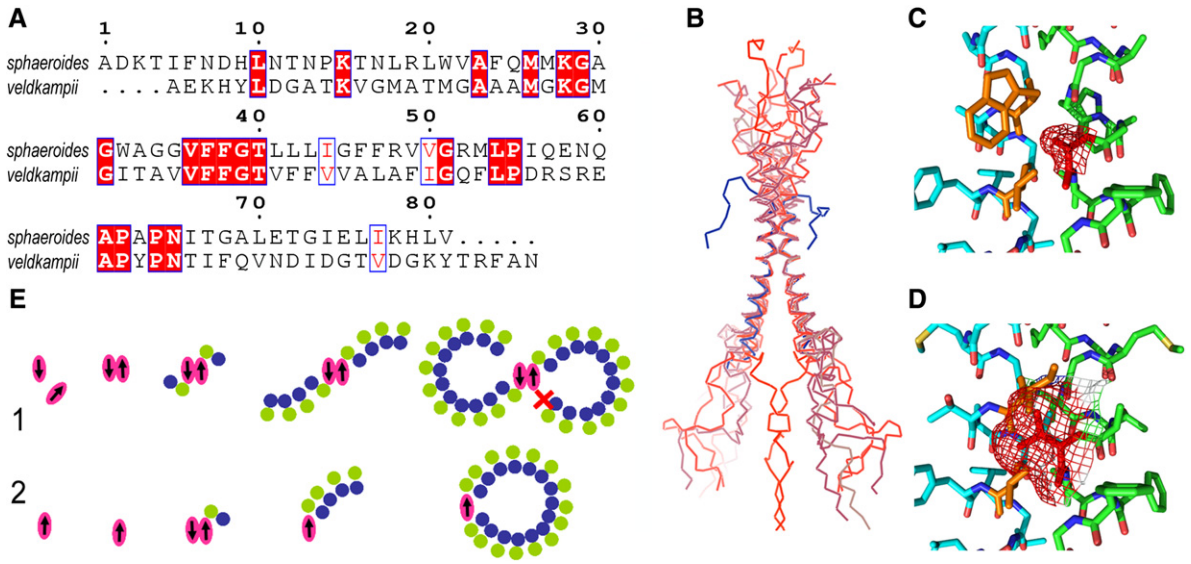

Figure 5. Dimerization of PufX Mediated through the $G_{31}XXXG_{35}$ Transmembrane Motif

(A) Sequence alignment of PufX from *Rba. sphaeroides* and *Rba. veldkampii*. The segment L_{18}-V_{50} of PufX from *Rba. sphaeroides* is α helix and contains a putatif $G_{31}XXXG_{35}$ dimerization motif.

(B) Seven dimers of PufX (in red) were built with the seven NMR conformers of monomeric PufX (PDB ID: 2DW3) and aligned with the dimer of glycophorin GpA (in blue) (see Experimental Procedures). The segments G_{29}-F_{38} are aligned with the GpA dimer, while deviations result from small bends of the PufX conformers. The dimers of PufX are depicted with the N termini facing upwards.

(C) A_{30}-F_{37} segment region of PufX from *Rba. sphaeroides* with G_{35} in red mesh.

(D) M_{30}-F_{37} segment region of PufX from *Rba. veldkampii* with V_{35} in red mesh, a substitution that destabilizes the dimer.

(E) Proposed model for the assembly of the subunits of the core complexes from *Rhodobacter* species. PufX and α and β subunits are depicted in pink, blue, and green, respectively. (1) In *Rba. sphaeroides*, following the biosynthesis of PufX, a dimer of PufX is formed, to which LH1 α/β pairs are assembled, leading to two LH1 rings of opposite curvature. Steric hindrance prevents a complete enclosure of the LH1. (2) In *Rba. veldkampii*, LH1 α/β pairs are assembled from a single PufX up to the point of LH1 ring closure.

has been found without any detectable dimers after purification by all procedures reported for the purification of the dimer of *Rba. sphaeroides* (Gubellini et al., 2006). Furthermore, the number of the resolved α/β pairs is 15, while the numbers of α/β pairs in a dissociated dimer would be 12 (Scheuring et al., 2004b), 13 (Abresch et al., 2005), or 14 (Qian et al., 2005) in *Rba sphaeroides* and 13 in *Rba. blasticus* (Scheuring et al., 2005b). Finally, when analyzed by AFM in the native membrane, the topographies of the core complex of *Rba. veldkampii* and of *Rba. blasticus* appeared strikingly different. In the former case, the LH1 analyzed at medium resolution presented a closed and circular LH1 (Milhiet et al., 2006). In the latter case, monomeric complexes likely resulting from the dissociation of the dimeric core complexes show an open C-shaped LH1 (Scheuring et al., 2005b). This suggests that in *Rba. veldkampii*, PufX is unable to induce the dimerization of the core complex.

The presence of PufX in the core complex has been determined biochemically through its partial sequencing, while the W subunit was shown to be absent in *Rba. veldkampii* (Gubellini et al., 2006). According to the putative sequence, PufX is expected to form a single transmembrane helix as for PufX of *Rba. sphaeroides* (Tsukatani et al., 2004). In the 3D reconstruction, densities that can be fitted with the structure of PufX from *Rba. sphaeroides* solved by NMR (Wang et al., 2007) are found in the opening and facing the Q_B site of the RC at the α inner ring level (Figure 4). This location of PufX is consistent with the role of PufX in the quinones exchange through the LH1 assembly in *Rba. veldkampii* (Gubellini et al., 2006) and in *Rba. sphaeroides* (Barz et al., 1995; Comayras et al., 2005a).

The transmembrane part of PufX contains a $G_{31}XXXG_{35}$ motif similar to the $G_{79}XXXG_{83}$ motif involved in the dimerization of the helical glycophorin GpA. This motif has been found in several proteins, and the interactions that hold together the dimer of GpA have been widely analyzed (for reviews, see Curran and Engelman [2003] and Senes et al. [2004]). In GpA, V_{84} also contributes to the stabilization of the dimer (Doura and Fleming, 2004) and in PufX, V_{36} is present at the equivalent position. We thus evaluated the formation of a dimer of PufX of *Rba. sphaeroides* and of *Rba. veldkampii* according to their sequence and the NMR structures (Figure 5A), keeping in mind that the NMR structures of *Rba. sphaeroides* were solved in organic solvent in which PufX is monomeric. We were unable to compute a dimer of PufX starting with the NMR conformers of PufX that had large bends (PDB ID: 2NRG) (Tunnicliffe et al., 2006). However, seven dimers of PufX-PufX could be built with the NMR conformers of PufX modeled as straight helices (PDB ID: 2DW3) (Wang et al., 2007) (rmsd of 0.6–1.45 Å for the G_{29}-F_{38} segment with the GpA dimer) (Figure 5B). These deviations are small and related to small differences in the curvature of

the PufX conformers. It is worth noting that in these dimers the bulky residues, e.g., W_{21}, F_{24}, W_{32}, F_{37}, and F_{38}, point outward in the dimer preventing steric hindrance between helices (data not shown).

In the *Rba. veldkampii* PufX sequence, the $G_{31}XXXV_{35}$ motif is present instead of $G_{31}XXXG_{35}$ in PufX of *Rba. sphaeroides*. Substitution of G_{35} with the bulkier V_{35} in the interface region of the dimer results in an overlap of the side chains that would lead to a steric hindrance, incompatible with the formation of a PufX-PufX dimer (Figures 5C and 5D). Furthermore, the equivalent position in GpA is G_{83}, and its substitution with several amino acids has been analyzed in detail by thermodynamical measurements and by the biochemical TOXCAT assay. It has been demonstrated that the substitution by a valine abolished the formation of dimer of GpA (Duong et al., 2007; Russ and Engelman, 2000).

This result suggest that dimerization of the core complexes from *Rhodobacter* species is mediated by the transmembrane domains of PufX. This conclusion is consistent with electron crystallographic studies of the dimeric core complex of *Rba. sphaeroides* (Scheuring et al., 2004b) and with AFM analysis of the dimeric core complex of *Rba. blasticus* (Scheuring et al., 2005b). From these studies, a model of the dimeric core complex has been proposed with a dimer of PufX present in the LH1 assembly and located at the core complex dimer junction (Scheuring et al., 2004b, 2005b). Finally, the transmembrane segment PufX of *Rba. capsulatus* is also capable of self-association, as analyzed by a TOXCAT (Aklujkar and Beatty, 2006).

A model involving PufX-PufX interaction mediated via their N termini has also been proposed (Qian et al., 2005). It is based on the projection map at 8.5 Å resolution from 2D crystals of LH1-RC from *Rba. sphaeroides* where two densities spaced by 90–100 Å were assigned to two PufX subunits. This distance appears too long for the unstructured N termini segments (A_1-A_{13}) if the structure of PufX as a straight α helix is considered (Wang et al., 2007). The NMR structure (PDB ID: 2NRG) reported a large bend in the Q_{15}-G_{32} segment of the α helix that is ~23 Å long and brings the N termini of PufX closer. Given a distance of ~3 Å between amino acids in an extended conformation, dimerization would be mediated by interaction between N termini segments of five to seven amino acids. While this hypothesis can not be ruled out, only two charged amino acids, K_4 and D_9, are present in the sequence of PufX from *Rba. sphaeroides*, as well as *Rba. veldkampii*, that could be involved in intermolecular electrostatic interactions.

A study of the time-dependent assembly of the photosynthetic unit has shown that the first subunits present in the native membrane are the PufX subunit, the H subunit of the RC, and the subunit IV of the cyt bc1, followed by the biosynthesis of the LH1 α/β polypeptides (Pugh et al., 1998). We proposed that following the synthesis of PufX from *Rba. sphaeroides*, a dimer of PufX is formed via the $G_{31}XXXG_{35}$ motif (Figure 5E, 1). Then, one LH1 α/β pair is assembled next at each side of the PufX dimer, and this is followed by others until the encircling of the RC. Due to the 2-fold axis of the PufX dimer and the nonequivalence of the α and β subunits, the assembly of LH1 α/β pairs leads to the formation of two antenna assemblies of opposite curvature that keep the α and the β subunits at their respective inner and the outer ring positions. The assembly of the LH1 α/β pairs is stopped by the steric hindrance of the PufX dimer and explains the two gaps in the dimeric LH1 assembly. In contrast, the stage-wise assembly of LH1 α/β pairs from the single PufX subunit, unable to dimerize like in *Rba. veldkampii*, leads to a single "gapped" monomeric core complex (Figure 5E, 2).

A $G_{101}XXXG_{105}$ motif has also been reported to be involved in the dimerization of the e subunit and the oligomerization of the mitochondrial ATP synthetase F_1F_O complexes. It is worth noting that deletion of the e subunit or single mutations that destabilize this motif have led to the loss of the long-range organization of F_1F_O in cristae in the mitochondria (Arselin et al., 2003; Bustos and Velours, 2005). In *Rba. sphaeroides*, the deletion of pufX that leads to the formation of a monomeric core complex also leads to the loss of the supramolecular organization of the core complexes in the membrane (Bahatyrova et al., 2004; Frese et al., 2000). The data reported here suggest that the destabilization of the $G_{31}XXXV_{35}$ motif in PufX, e.g., by the substitution of G_{35} as in *Rba. veldkampii*, would lead to a random organization of the core complexes from *Rhodobacter species* in the membrane.

EXPERIMENTAL PROCEDURES

Bacterial Strain, Growth Conditions, and Membrane Preparation

Rba. veldkampii strain DSM 11550 (from the German Strain Collection of Microorganisms and Cell Culture, DSMZ, Braunschweig, Germany) was grown for 72 hr (OD_{670nm} = 4 Abs) under photosynthetic conditions. Chromatophores were prepared as previously described (Gubellini et al., 2006). Briefly, cells were disrupted by French Press and centrifuged to remove unbroken cells. The supernatant was ultracentrifuged in a Beckman rotor type 45 Ti for 1 hr 30 min at 125,000 × g (4°C), resuspended in 50 mM glygly (pH 7.8), EDTA 1 mM, benzoamidine 1 mM, and immediately frozen.

Isolation and Purification of the Core Complexes

Membranes were solubilized for 15 min at 4°C in the dark in 3.5% n-dodecyl-β-D-thiomaltopyranoside (DOTM), and the photosynthetic complexes were separated on a linear gradient of 11%–33% w/w sucrose in 50 mM gly-gly (pH 7.6), 0.1% DOTM (Gubellini et al., 2006). The core complexes were extracted and further purified by a DEAE column to remove any trace of LH2. Finally, core complexes were purified by size-exclusion chromatography in 50 mM Gly-Gly (pH 7.6), 0.1% DOTM. The H, L, and M subunits of the RC, the α and β subunits from the LH1, and the PufX subunit were separated in a 17% acrylamide SDS-PAGE and silver stained. It is worth noting that no additional band was found in the 50–6 kDa region that could reveal the presence of an additional peptide. The putative band of PufX was cut from the gel and assigned as PufX after analysis by MALDI/MS and by ES Q-Tof MS/MS analysis. Concentration of the purified core complex (final ratio Abs_{880nm}/Abs_{280nm} of 1.9) was calculated with an extinction coefficient of 3.9 $\mu M^{-1}cm^{-1}$ at 884 nm as in *Rb. sphaeroides* (Francia et al., 2004).

Electron Microscopy

For cryo-EM analysis, proteins concentrated at 1.5 mg/ml were flash frozen in liquid ethane. Cryo-images were recorded in a Jeol 2010 FEG microscope operating at 200 kV under low-dose conditions at a nominal magnification of 45,000×, with a 1.3–3.5 μm defocus range. Micrographs were digitized with a Nikon Coolscan 8000ED densitometer with a final pixel size of 1.95 Å/pixel. The magnification was calibrated with TMV virus.

3D Reconstruction from Cryo-Images

A total of 44,000 particles were semiautomatically picked with Boxer algorithm of EMAN package. Each particle defocus was estimated from the defocus of the micrograph, calculated with ctftilt (Mindell and Grigorieff, 2003), and from its coordinates on the micrograph. For CTF correction, eight groups of homogeneous defocus were constructed leading to a selection of 27,000 particles. The near atomic structure of core complex of *Rps. palustris* (PDB ID: 1PYH) was strongly low-pass filtered at 25 Å, to prevent alignment bias, and used only once, to provide a rough first estimate of the orientations corresponding to our images. Thenceforth, *Rba veldkampii* images were iteratively aligned on their own, by using the 3D projection-matching algorithm (Penczek et al., 1994; Radermacher, 1994) with Wiener filtration (Grigorieff, 1998). Refinements converged to a stable CTF corrected 3D reconstruction with a resolution estimated at 1/12 $Å^{-1}$ by the $FSC_{0.5}$ criterion.

Two other volumes were built and used as a reference volume for 3D projection matching but failed to produce a stable 3D reconstruction: a volume of *Rps. palustris* with a LH1 ring closed with an additional α/β pair i.e., with a 16 α/β LH1 and filtered at 25 Å as above, and a second volume constructed from a synthetic circular ring surrounding the RC from *Rba. sphaeroides* filtered at 25 Å.

Classification of the 44,000 cryo-images projection images was performed through multireference alignment with 92 directions of projection corresponding to an angular step of 20° of the final 3D reconstruction volume of *Rba. veldkampii*. Hence, images matching the 2D projections of the volume were used to compute 92 specific class averages (Figure 1E). The coherence of the 3D reconstruction was evaluated by comparison of 2D projections of the volume with the class averages and by the fitting of the RC of *Rba. sphaeroides* (PDB ID: 1PSS) in the EM volume with the SITUS package (Wriggers et al., 1999). The threshold of the 3D reconstruction depicted in Figure 4 (purple surface) has been adjusted according to a mass of 280 kDa, i.e., the molecular weight of the core complex without the nonresolved bacteriochlorophylls, and an average density of 0.81 Da. $Å^{-3}$ with Chimera software. The brown threshold corresponds to a threshold slightly above the noise appearing outside the 3D reconstruction and without additional noise on the RC and LH1 subunits.

The X-mipp package (Sorzano et al., 2004) was used for all 2D-image processing and SPIDER software (Frank et al., 1996) for multivariate statistical analysis, multireference alignment, 3D reconstructions, and CTF correction.

Structure Modeling

The structure of a dimer of PufX from *Rba. sphaeroides* was built with the PyMOL software (DeLano Scientific, LLC) by using NMR structures of the PufX monomer (PDB ID: 2DW3 [Wang et al., 2007] or PDB ID: 2ITA and PDB ID: 2NRG [Tunnicliffe et al., 2006]) and the NMR structure of the dimer of glycophorin GpA (PDB ID: 1AFO). For all conformers of both NMR structure of PufX (Wang et al., 2007), the backbones of the G_{29}-F_{38} segments that contain the putative $G_{31}XXXG_{35}$ dimerization motif were selected and structurally aligned with the backbone of chain A of GlpA. The segments were duplicated and aligned with chain B of GlpA. No matching was found with the GpA structure when NMR structures of PufX 2ITA and 2NRG were used, likely due to the curvature of the structure. However, by using the seven conformers of the PufX structure PDB ID 2DW3, the backbones were aligned with rmsd ranging from 1.45 Å (conformer 1) to 0.61 Å (conformer 5). These alignments were used to generate seven dimers of PufX that were compared with the dimer of GpA with final rmsd ranging from 1.44Å (dimer of conformers 1) to 0.62 Å (dimer of conformers 5). The substitution of G_{35} present in PufX of *Rba. sphaeroides* to V_{35} of *Rba. veldkampii* was analyzed with PyMOL.

ACKNOWLEDGMENTS

This study was supported by the European Community (IHP-RTN), the Human Frontier Science Program (to F.G.), the Ministère de la Recherche Française (to J.B.), the European Commission for NoE 3DEM (contract number LSHG-CT-2004-502828) (to M.C.), the Agence Nationale de la Recherche (contract number PCV06-135175) (to D.L.), the Curie Institut, and the Centre National de la Recherche Scientifique. The cryo-EM images were taken with the "Fédératif" FEG microscope at the Pasteur Institut with the appreciate help of G. Pehau-Arnaudet. Dr. Z. Wang is warmly thanked for providing the NMR coordinates of the structure of PufX and Dr. S. Marco and Dr. S. Jovic for fruitful discussions. The authors declare that the manuscript has been submitted without any potential conflicts of interest.

Received: May 9, 2007
Revised: September 19, 2007
Accepted: September 20, 2007
Published: December 11, 2007

REFERENCES

Abresch, E.C., Axelrod, H.L., Beatty, J.T., Johnson, J.A., Nechushtai, R., and Paddock, M.L. (2005). Characterization of a highly purified, fully active, crystallizable RC-LH1-PufX core complex from *Rhodobacter sphaeroides*. Photosynth. Res. *86*, 61–70.

Aird, A., Wrachtrup, J., Schulten, K., and Tietz, C. (2007). Possible pathway for ubiquinone shuttling in *Rhodospirillum rubrum* revealed by molecular dynamics simulation. Biophys. J. *92*, 23–33.

Aklujkar, M., and Beatty, J.T. (2006). Investigation of *Rhodobacter capsulatus* PufX interactions in the core complex of the photosynthetic apparatus. Photosynth. Res. *88*, 159–171.

Allen, J.P., Feher, G., Yeates, T.O., Komiya, H., and Rees, D.C. (1987). Structure of the reaction center from *Rhodobacter sphaeroides* R-26: the cofactors. Proc. Natl. Acad. Sci. USA *84*, 5730–5734.

Arselin, G., Giraud, M., Dautant, A., Vaillier, J., Brethes, D., Coulary-Salin, B., Schaeffer, J., and Velours, J. (2003). The GxxxG motif of the transmembrane domain of subunit e is involved in the dimerization/oligomerization of the yeast ATP synthase complex in the mitochondrial membrane. Eur. J. Biochem. *270*, 1875–1884.

Bahatyrova, S., Frese, R.N., Siebert, C.A., Olsen, J.D., Van Der Werf, K.O., Van Grondelle, R., Niederman, R.A., Bullough, P.A., Otto, C., and Hunter, C.N. (2004). The native architecture of a photosynthetic membrane. Nature *430*, 1058–1062.

Baker, T.S., and Cheng, R.H. (1996). A model-based approach for determining orientations of biological macromolecules imaged by cryoelectron microscopy. J. Struct. Biol. *116*, 120–130.

Barz, W.P., Francia, F., Venturoli, G., Melandri, B.A., Vermeglio, A., and Oesterhelt, D. (1995). Role of PufX protein in photosynthetic growth of *Rhodobacter sphaeroides*. 1. PufX is required for efficient light-driven electron transfer and photophosphorylation under anaerobic conditions. Biochemistry *34*, 15235–15247.

Berry, E.A., Huang, L.S., Saechao, L.K., Pon, N.G., Valkova-Valchanova, M., and Daldal, F. (2004). X-ray structure of *Rhodobacter capsulatus* cytochrome bc (1): comparison with its mitochondrial and chloroplast counterparts. Photosynth. Res. *81*, 251–275.

Bustos, D.M., and Velours, J. (2005). The modification of the conserved GXXXG motif of the membrane-spanning segment of subunit g destabilizes the supramolecular species of yeast ATP synthase. J. Biol. Chem. *280*, 29004–29010.

Chen, S., Roseman, A.M., Hunter, A.S., Wood, S.P., Burston, S.G., Ranson, N.A., Clarke, A.R., and Saibil, H.R. (1994). Location of a folding protein and shape changes in GroEL-GroES complexes imaged by cryo-electron microscopy. Nature *371*, 261–264.

Comayras, F., Jungas, C., and Lavergne, J. (2005a). Functional consequences of the organization of the photosynthetic apparatus in *Rhodobacter sphaeroides*. I. Quinone domains and excitation transfer in chromatophores and reaction center.antenna complexes. J. Biol. Chem. *280*, 11203–11213.

Comayras, F., Jungas, C., and Lavergne, J. (2005b). Functional consequences of the organization of the photosynthetic apparatus in *Rhodobacter sphaeroides*: II. A study of PufX- membranes. J. Biol. Chem. *280*, 11214–11223.

Crowther, R.A. (1971). Procedures for three-dimensional reconstruction of spherical viruses by Fourier synthesis from electron micrographs. Philos. Trans. R. Soc. Lond. B Biol. Sci. *261*, 221–230.

Curran, A.R., and Engelman, D.M. (2003). Sequence motufs, polar interactions and conformational changes in helical membrane proteins. Curr. Opin. Struct. Biol. *13*, 412–417.

Deisenhofer, J., Epp, O., Miki, K., Huber, R., and Michel, H. (1984). X-ray structure analysis of a membrane protein complex. Electron density map at 3 Å resolution and a model of the chromophores of the photosynthetic reaction center from *Rhodopseudomonas viridis*. J. Mol. Biol. *180*, 385–398.

Doura, A.K., and Fleming, K.G. (2004). Complex interactions at the helix-helix interface stabilize the glycophorin A transmembrane dimer. J. Mol. Biol. *343*, 1487–1497.

Duong, M.T., Jaszewski, T.M., Fleming, K.G., and MacKenzie, K.R. (2007). Changes in apparent free energy in helix-helix dimerization in a biological membrane due to point mutations. J. Mol. Biol. *371*, 422–434.

Francia, F., Dezi, M., Rebecchi, A., Mallardi, A., Palazzo, G., Melandri, B.A., and Venturoli, G. (2004). Light-harvesting complex 1 stabilizes P+QB- charge separation in reaction centers of *Rhodobacter sphaeroides*. Biochemistry *43*, 14199–14210.

Francia, F., Wang, J., Venturoli, G., Melandri, B.A., Barz, W.P., and Oesterhelt, D. (1999). The reaction center-LH1 antenna complex of *Rhodobacter sphaeroides* contains one PufX molecule which is involved in dimerization of this complex. Biochemistry *38*, 6834–6845.

Frank, J., Radermacher, M., Penczek, P., Zhu, J., Li, Y., Ladjadj, M., and Leith, A. (1996). SPIDER and WEB: processing and visualization of images in 3D electron microscopy and related fields. J. Struct. Biol. *116*, 190–199.

Frese, R.N., Olsen, J.D., Branvall, R., Westerhuis, W.H., Hunter, C.N., and van Grondelle, R. (2000). The long-range supraorganization of the bacterial photosynthetic unit: a key role for PufX. Proc. Natl. Acad. Sci. USA *97*, 5197–5202.

Gelfand, M.S., and Goncharov, A.B. (1989). Spatial rotational alignment of identical particles in the case of (almost) coaxial projections. Ultramicroscopy *27*, 301–306.

Ghosh, R., Ghosh-Eisher, S., DiBernardino, M., and Bachofen, R. (1994). Protein phosphorylation in *Rhodospirulum rubrum*: purification and characterization of a water soluble B873 protein kinase and a new component of the B873 complex, omega, which can be phosphorylated. Biochim. Biophys. Acta *1184*, 28–36.

Grigorieff, N. (1998). Three-dimensional structure of bovine NADH:ubiquinone oxidoreductase (complex I) at 22 A in ice. J. Mol. Biol. *277*, 1033–1046.

Gubellini, F., Francia, F., Busselez, J., Venturoli, G., and Levy, D. (2006). Functional and structural analysis of the photosynthetic apparatus of *Rhodobacter veldkampii*. Biochemistry *45*, 10512–10520.

Jamieson, S.J., Wang, P., Qian, P., Kirkland, J.Y., Conroy, M.J., Hunter, C.N., and Bullough, P.A. (2002). Projection structure of the photosynthetic reaction centre-antenna complex of *Rhodospirillum rubrum* at 8.5 Å resolution. EMBO J. *21*, 3927–3935.

Joliot, P., Joliot, A., and Vermeglio, A. (2005). Fast oxidation of the primary electron acceptor under anaerobic conditions requires the organization of the photosynthetic chain of *Rhodobacter sphaeroides* in supercomplexes. Biochim. Biophys. Acta *1706*, 204–214.

Jungas, C., Ranck, J.L., Rigaud, J.L., Joliot, P., and Vermeglio, A. (1999). Supramolecular organization of the photosynthetic apparatus of *Rhodobacter sphaeroides*. EMBO J. *18*, 534–542.

Karrasch, S., Bullough, P.A., and Ghosh, R. (1995). The 8.5 Å projection map of the light-harvesting complex I from *Rhodospirillum rubrum* reveals a ring composed of 16 subunits. EMBO J. *14*, 631–638.

Koepke, J., Hu, X., Muenke, C., Schulten, K., and Michel, H. (1996). The crystal structure of the light-harvesting complex II (B800–850) from *Rhodospirillum molischianum*. Structure *4*, 581–597.

Leschziner, A.E., and Nogales, E. (2006). The orthogonal tilt reconstruction method: an approach to generating single-class volumes with no missing cone for ab initio reconstruction of asymmetric particles. J. Struct. Biol. *153*, 284–299.

Ludtke, S.J., Baldwin, P.R., and Chiu, W. (1999). EMAN: semiautomated software for high-resolution single-particle reconstructions. J. Struct. Biol. *128*, 82–97.

Milhiet, P.E., Gubellini, F., Berquand, A., Dosset, P., Rigaud, J.L., Le Grimellec, C., and Levy, D. (2006). High-resolution AFM of membrane proteins directly incorporated at high density in planar lipid bilayer. Biophys. J. *91*, 3268–3275.

Mindell, J.A., and Grigorieff, N. (2003). Accurate determination of local defocus and specimen tilt in electron microscopy. J. Struct. Biol. *142*, 334–347.

Nogi, T., Fathir, I., Kobayashi, M., Nozawa, T., and Miki, K. (2000). Crystal structures of photosynthetic reaction center and high-potential iron-sulfur protein from *Thermochromatium tepidum*: thermostability and electron transfer. Proc. Natl. Acad. Sci. USA *97*, 13561–13566.

Papiz, M.Z., Hawthornthwaite, A.M., Cogdell, R.J., Woolley, K.J., Wightman, P.A., Ferguson, L.A., and Lindsay, J.G. (1989). Crystallization and characterization of two crystal forms of the B800–850 light-harvesting complex from *Rhodopseudomonas acidophila* strain 10050. J. Mol. Biol. *209*, 833–835.

Parkes-Loach, P.S., Majeed, A.P., Law, C.J., and Loach, P.A. (2004). Interactions stabilizing the structure of the core light-harvesting complex (LH1) of photosynthetic bacteria and its subunit (B820). Biochemistry *43*, 7003–7016.

Penczek, P.A., Grassucci, R.A., and Frank, J. (1994). The ribosome at improved resolution: new techniques for merging and orientation refinement in 3D cryo-electron microscopy of biological particles. Ultramicroscopy *53*, 251–270.

Pugh, R.J., McGlynn, P., Jones, M.R., and Hunter, C.N. (1998). The LH1-RC core complex of *Rhodobacter sphaeroides*: interaction between components, time-dependent assembly, and topology of the PufX protein. Biochim. Biophys. Acta *1366*, 301–316.

Qian, P., Hunter, C.N., and Bullough, P.A. (2005). The 8.5 Å projection structure of the core RC-LH1-PufX dimer of *Rhodobacter sphaeroides*. J. Mol. Biol. *349*, 948–960.

Radermacher, M. (1994). Three-dimensional reconstruction from random projections: orientational alignment via Radon transforms. Ultramicroscopy *53*, 121–136.

Radermacher, M., Wagenknecht, T., Verschoor, A., and Frank, J. (1987a). Three-dimensional reconstruction from a single-exposure, random conical tilt series applied to the 50S ribosomal subunit of *Escherichia coli*. J. Microsc. *146*, 113–136.

Radermacher, M., Wagenknecht, T., Verschoor, A., and Frank, J. (1987b). Three-dimensional structure of the large ribosomal subunit from *Escherichia coli*. EMBO J. *6*, 1107–1114.

Roszak, A.W., Howard, T.D., Southall, J., Gardiner, A.T., Law, C.J., Isaacs, N.W., and Cogdell, R.J. (2003). Crystal structure of the RC-LH1 core complex from *Rhodopseudomonas palustris*. Science *302*, 1969–1972.

Russ, W.P., and Engelman, D.M. (2000). The GxxxG motif: a framework for transmembrane helix-helix association. J. Mol. Biol. *296*, 911–919.

Scheuring, S., and Sturgis, J.N. (2005). Chromatic adaptation of photosynthetic membranes. Science *309*, 484–487.

Scheuring, S., Seguin, J., Marco, S., Levy, D., Robert, B., and Rigaud, J.L. (2003). Nanodissection and high-resolution imaging of the *Rhodopseudomonas viridis* photosynthetic core complex in native membranes by AFM. Atomic force microscopy. Proc. Natl. Acad. Sci. USA *100*, 1690–1693.

Scheuring, S., Rigaud, J.L., and Sturgis, J.N. (2004a). Variable LH2 stoichiometry and core clustering in native membranes of *Rhodospirillum photometricum*. EMBO J. *23*, 4127–4133.

Scheuring, S., Francia, F., Busselez, J., Melandri, B.A., Rigaud, J.L., and Levy, D. (2004b). Structural role of PufX in the dimerization of the photosynthetic core complex of *Rhodobacter sphaeroides*. J. Biol. Chem. *279*, 3620–3626.

Scheuring, S., Lévy, D., and Rigaud, J.L. (2005a). Watching the components of photosynthetic bacterial membranes and their in situ organization by atomic force microscopy. Biochim. Biophys. Acta *1712*, 109–127.

Scheuring, S., Busselez, J., and Levy, D. (2005b). Structure of the dimeric PufX-containing core complex of *Rhodobacter blasticus* by in situ atomic force microscopy. J. Biol. Chem. *280*, 1426–1431.

Scheuring, S., Goncalves, R.P., Prima, V., and Sturgis, J.N. (2006). The photosynthetic apparatus of *Rhodopseudomonas palustris*: structures and organization. J. Mol. Biol. *358*, 83–96.

Senes, A., Engel, D.E., and DeGrado, W.F. (2004). Folding of helical membrane proteins: the role of polar, GXXXG-like and proline motifs. Curr. Opin. Struct. Biol. *14*, 465–479.

Siebert, C.A., Qian, P., Fotiadis, D., Engel, A., Hunter, C.N., and Bullough, P.A. (2004). Molecular architecture of photosynthetic membranes in *Rhodobacter sphaeroides*: the role of PufX. EMBO J. *23*, 690–700.

Sorzano, C.O., Marabini, R., Velazquez-Muriel, J., Bilbao-Castro, J.R., Scheres, S.H., Carazo, J.M., and Pascual-Montano, A. (2004). XMIPP: a new generation of an open-source image processing package for electron microscopy. J. Struct. Biol. *148*, 194–204.

Tsukatani, Y., Matsuura, K., Masuda, S., Shimada, K., Hiraishi, A., and Nagashima, K.V. (2004). Phylogenetic distribution of unusual triheme to tetraheme cytochrome subunit in the reaction center complex of purple photosynthetic bacteria. Photosynth. Res. *79*, 83–91.

Tunnicliffe, R.B., Ratcliffe, E.C., Hunter, C.N., and Williamson, M.P. (2006). The solution structure of the PufX polypeptide from *Rhodobacter sphaeroides*. FEBS Lett. *580*, 6967–6971.

Wang, Z.Y., Suzuki, H., Kobayashi, M., and Nozawa, T. (2007). Solution structure of the *Rhodobacter sphaeroides* PufX membrane protein: implications for the quinone exchange and protein-protein interactions. Biochemistry *46*, 3635–3642.

Wriggers, W., Milligan, R.A., and McCammon, J.A. (1999). Situs: a package for docking crystal structures into low-resolution maps from electron microscopy. J. Struct. Biol. *125*, 185–195.

Yan, X., Dryden, K.A., Tang, J., and Baker, T.S. (2007). Ab initio random model method facilitates 3D reconstruction of icosahedral particles. J. Struct. Biol. *157*, 211–225.

Accession Numbers

The 3D reconstruction has been deposited in the Macromolecular Structure Data Base, submission number EM-1356.